Nat Hazards (2016) 81:1229–1247
DOI 10.1007/s11069-015-2131-x

ORIGINAL PAPER

Laboratory study on protection of tsunami-induced scour by offshore breakwaters

Jie Chen[1,2] · Changbo Jiang[1,2] · Wu Yang[1] · Guizhen Xiao[1]

Received: 11 May 2015 / Accepted: 13 December 2015 / Published online: 24 December 2015

Abstract Devastating tsunami waves can mobilize substantial amount of coastal sediment. Scouring is the primary damage caused by tsunamis. Offshore submerged or emerged breakwaters are coastal structures that are commonly employed to provide protection to valuable coastal beaches from energetic ocean waves. However, the protection capabilities of tsunami scour by submerged or emerged breakwater are less understood compared to tsunami runup and tsunami inundation. A set of laboratory experiments are reported in this study on protection of tsunami-induced scour by submerged or emerged breakwaters on a sandy beach. FLOW-3D is used in this paper to calculate flow field of tsunami wave propagation over the breakwater in order to help us to understand the sediment transport and tsunami scour process. Our experiments show that the submerged breakwater could not effectively reduce the tsunami scouring and only could affect the height and position of deposition sand bar. The emerged breakwater could significantly effectively reduce the tsunami scouring on the sandy beach; meanwhile, local scouring caused by plunging jet occurs mainly on the both sides of the structure. It is also found that for typical tsunamis, the scour depth at shoreward is unlikely to reach its equilibrium stage. Local scouring damage is one of the main factors leading to the destruction of coastal structures during a tsunami event. The most important governing parameters on local scouring around breakwater were defined. The final empirical relations that define the magnitude and position of local scouring around the breakwater were presented. The information reported in this study is useful for local authorities to assess potential tsunami damage of structure and to have a better plan for tsunami preventing and reducing.

✉ Changbo Jiang
Jcb36@vip.163.com

Jie Chen
chenjie166@163.com

[1] School of Hydraulic Engineering, Changsha University of Science and Technology, Changsha 410114, People's Republic of China

[2] Hunan Province Key Laboratory of Water, Sediment Sciences and Flood Hazard Prevention, Changsha 410114, People's Republic of China

Keywords Tsunami scour · Tsunami wave · Emerged breakwater · Submerged breakwater · Experimental study · FLOW-3D

1 Introduction

Tsunami scour has received increasing attention over the past decade, given that it produces significant erosion in affected coastal areas, and in particular the wide-scale damage to infrastructure resulting from the 2004 Sumatra Andaman Tsunami and the 2011 Tohoku Tsunami. Tsunami waves with the height of 5–10 m will be inevitably accompanied by very high flow velocities when they penetrate inland, which will undoubtedly produce high bed shear stresses and a mount of sediment movements over large areas, resulting in substantial beach erosion and scouring around a large number of structures (Li et al. 2012). The resulting scour damage can undermine building foundations, roadways, embankments, underground pipelines, and other coastal structures. To reduce future potential economical losses in coastal areas prone to devastating tsunamis, it is crucial to understand and to predict geomorphical changes associated with tsunamis to guide future planning, design, and development of coastlines and coastal infrastructures. It is also vital to understand sediment transport processes under complex tsunami wave conditions for predicting potential tsunami hazards in the future.

Tsunami wave-induced sediment transport processes on sandy beach have been studied very little in comparison with a large number of studies performed for those under waves and currents. Although the mechanisms for scour formation under tsunami loading seem similar to those induced by storm-generated waves, there are some differences. Storm waves have many cycles with a period of less than tens of seconds. Tsunamis typically have one or a few cycles with a period in minutes or tens of minutes.

Currently, there exist a limited number of laboratory studies of tsunami erosion and deposition processes. Kobayashi and Lawrence (2004) reported a laboratory study of beach profile changes under solitary waves. Alsina et al. (2009) studied, experimentally and numerically, characteristics of suspended sand caused by breaking solitary waves. Tsujimoto et al. (2008) measured the beach profile changes under solitary waves alone and in combination with regular waves. Young et al. (2010) performed a large-scale experimental study to examine the cross-shore sediment transport as well as erosion and deposition patterns of a near-equilibrium sand beach under the action of about 100 solitary and cnoidal waves of small height. Sumer et al. (2011) reported a detailed study of sediment transport induced by a plunging solitary wave. Chen et al. (2012) performed laboratory experiments to investigate the changes of beach profile and mean sand grain size by tsunami-like waves. The above experimental results all show that a tsunami is capable of causing sediment motion in both the uprush and backwash phases and that the backwash process mainly by sheet flow is stronger than the uprush.

On the other hand, a few laboratory studies focus on tsunami scour around the structure. Kato et al. (2000) and Tonkin et al. (2003) performed large-scale model experiments on tsunami-induced scouring mechanisms around a cylindrical structure on a flat beach. Nakamura et al. (2008, 2009) investigated, experimentally and numerically, the tsunami-induced local scour around a land-based square structure on a sand foundation. Ca et al. (2000) investigated coastal scour and erosion due to tsunami backflow. Chen et al. (2013) performed an experimental study on tsunami-induced scour at a road model situated on a

sandy beach. The above experiments reveal that the most rapid scour on sand substrate occurred during the tsunami backwash stage. However, most of their studies focus on tsunami scour processes and scour depth, and current knowledge about how to protect and decrease tsunami-induced scour is still limited and yet to be investigated.

Coastal structures located within or just seaward of the surf zone are often meant to limit shoreline erosion, or to promote beach widening by the formation of a salient. Offshore breakwaters are common coastal structures that are employed to provide protection to valuable coastal beaches from energetic ocean wave. The primary functions of offshore breakwaters are to cause waves to prematurely break, to reduce the amount of wave energy in their lee, and to initiate sediment deposition at the shoreline. Traditionally, emerged offshore breakwaters, whose crest pierces the mean water level, have been used to accomplish this task in the USA and Europe (Dean and Dalrymple 2001), and even more so in Japan, where Seiji et al. (1987) reported the completion of over 4000 emergent offshore breakwaters by the mid-1980s. Recently, submerged offshore breakwaters, which lie entirely beneath the mean water level, have become more common and only rarely been adopted for beach protection.

While some investigations suggest that emerged offshore breakwaters could perform well for coastal protection under storm events, other investigations indicate that submerged offshore breakwaters are widely perceived to be capable of providing beach protection, without the adverse impacts (including loss of beach amenity and esthetic considerations). In contrast, protection of tsunami-induced erosion and scour are very few reported in the offshore breakwaters, including emerged and submerged. It is certainty that the characteristics of and processes governing shoreline response to storm surge and tsunami wave, emerged and submerged offshore breakwaters, are fundamentally different. As such, some well established methods that are currently used to predict shoreline response to offshore breakwaters under storm events (e.g., empirical relationships) may not be suitable to investigate shoreline response to offshore breakwaters under tsunami wave. The offshore breakwaters, including emerged or submerged, could be capable of providing protection for tsunami scour is an interrogatory. Therefore, prior to the wider adoption of offshore breakwaters for beach protection, it is imperative that an extensive study be undertaken to rigorously investigate characteristics of and processes governing shoreline response to offshore breakwaters under tsunami wave.

The objectives of this study are: (1) to understand how beach profiles are affected by emerged and submerged offshore breakwater under tsunami wave actions; (2) to analyze offshore breakwater effects on wave hydrodynamics and associated sediment transport; and (3) to investigate protection capability of tsunami-induced scour by offshore breakwater. Therefore, this paper is organized as follows: Firstly, the experimental set-up and test procedures are detailed in Sect. 2. In laboratory studies, there is too much difficulty in measuring the flow field of tsunami wave propagation to the breakwater, partly due to fact that the commonly used acoustic Doppler velocimeter is single-point measurement, and partly due to fact that the particle image velocimetry (PIV) is unable to measure the flow field with sediment movement. FLOW-3D is general-purpose computational fluid dynamics (CFD) software. It employs specially developed numerical techniques to solve the equations of motion for fluids to obtain transient, three-dimensional solutions to multi-scale, multi-physics flow problems. FLOW-3D is used in this paper to calculate flow field of tsunami wave propagation over the breakwater, which could help us to understand the sediment transport and tsunami scour process. The model validation is then presented in Sect. 3. The morphological response of beach profiles affected by emerged and submerged offshore breakwater under tsunami wave actions is respectively described in Sect. 4.

Finally, Sect. 5 discusses previous observations reported in the literature and brings out the main ideas of this study.

2 Experimental setup and test procedure

Following Chen et al. (2012), further experiments were conducted in a two-dimensional (2D) glass-walled wave flume in the hydraulics laboratory in Changsha University of Science and Technology, P. R. China. The wave flume was 40.0 m long, 0.5 m wide, and 0.8 m high. A piston-type wave maker was installed at one end of the flume, and a sand beach was constructed on the other side of the flume.

One of the difficulties in studying tsunami-induced sediment transport under laboratory conditions lies in downscaling the tsunami flows (very long waves) and sand grains in physical modeling. We remark that it is difficult to model tsunami waves in a wave flume using a geometric similarity: Because of the limitation of the flume length, the modeled tsunami waves in a wave flume are inevitably much steeper than real tsunami waves. Therefore, a geometrically distorted model is unavoidable in the laboratory studies of tsunami-related problems. In general, tsunami waves may take many shapes, but typically take the form of individual solitary waves, rather than periodic waves. Solitary waves have been used in experimental study as a proxy for tsunami wave forms in most cases (e.g., Goring 1979; Synolakis and Bernard 2006), although the accuracy of this approximation is extensively discussed by Madsen et al. (2008). It is possible to generate solitary waves whose waveform is qualitatively similar to that of typical tsunami waves, both the length and time scales of actual tsunami waves cannot be downscaled in wave flume experiments according to Froude similarity law.

The scaling effects of small-scale sediment transport laboratorial experiments are probably significant, since normally the sand substrate must be modeled at full scale, while the tsunami waves are modeled at reduced scale. Very fine sediments cannot be used as a scale model of sand, since finer sediments tend to become cohesive (Tonkin et al. 2003). So the natural sand was used in existing tsunami sediment experimental research (such as Kato et al. 2000; Tonkin et al. 2003; Young et al. 2010; Kobayashi and Lawrence 2004; Chen et al. 2012, 2013; Jiang et al. 2015). Because natural sand is used in our experiments, the wave height needs to be selected, so the flow can move the sand grains. To select appropriate wave heights for the experiments, we make the following order-of-magnitude estimation. The flow depth when water rushes up the beach can be estimated by βH, with H being the incoming wave height and $0 < \beta < 1$; as a result, the mean velocity of the flow rushing up the beach can be estimated by $U = \alpha\sqrt{gH}$ where g is the gravitational acceleration and $0 < \alpha < \sqrt{\beta}$. The above estimation can be partly verified by the observed mean speed of the wave front, which was of $O(0.5$ m/s) in our experiments. The friction velocity can be estimated by $u_* = \alpha f\sqrt{gH}$, with f being a friction factor for the sand beach. For $H = 0.15$ m, $f = 0.2$, and $\alpha = 0.5$, $u_* = O(0.12$ m/s) is obtained, and the grain Reynolds number (defined by $Re_* = u_* d_s/\nu$, with d_s being the grain diameter and ν the viscosity of water) is of $O(20)$ for the 0.30-mm sand grains. The critical Shields parameter, defined by $\theta_c = u_{*c}^2/[gd_s(s-1)]$,with u_{*c} being the critical shear velocity and s the ratio of sand grain density to water density, is about 0.04 for 0.30-mm sand grains. Therefore, the critical shear velocity u_{*c} should be of $O(0.014$ m/s) for the 0.3-mm sand grains, and long waves with a height of $H = O(0.05$ m) should be able to move the sand grains used in our

experiments. The flow velocity that can be achieved in our wave flume is an order of magnitude smaller than that of typical tsunami flows.

Because natural sand was used in our experiments and the flow generated in the wave flume was much weaker than tsunami flows in field conditions, the Shields parameter in our experiments was generally much smaller than that for tsunami flows. The insufficient Shields parameter could be offset to a certain extent by running identical solitary waves multiple times, as done in Kobayashi and Lawrence (2004), Young et al. (2010), Chen et al. (2012, 2013) and Jiang et al. (2015). Running identical solitary waves multiple times also allows us to study the evolution of the sand beach under wave attacks.

For the convenience of describing the sand beach and the arrangement of the measuring devices, we define a Cartesian coordinate as follows: The x-axis points toward the sand beach with its origin being located at the toe of the sand beach, the z-axis points upward with its origin at the flume bottom, and the y-axis is perpendicular to the side wall of the flume with its origin at the inner surface of the front side of the flume.

Referring to Fig. 1, the slope of the sand beach changed from 1/10–1/20 at $x = 3.5$ m, and the 1/20 slope was 4.0 m long. The sand beach was constructed using the well-sorted natural sand. Sieve analysis was performed on the three different random sand samples. The sand had a mean median diameter $d_{50} = 0.368$ mm. The mean coefficient of uniformity ($C_u = d_{60}/d_{10}$) for this sand was calculated as 2.83, and the mean coefficient of curvature ($C_c = d_{30}^2/(d_{10}d_{60})$) was calculated as 1.11.

A series of solitary waves was selected as incident wave in the flume. The wave height H was 0.15 m, and the water depth h was 0.35 m. The test conditions examined in the experiments are listed in Table 1.

Referring to Fig. 1 (top panel), the submerged breakwater model, which was a 10.0-cm crest wide rectangle cement blockwork, was located in the middle of slope from $x = 1.75$ m to $x = 2.50$ m. The depth of submergence R was 5.0 cm, 8.0 cm and 10.0 cm respectively. Referring to Fig. 1 (bottom panel), the emerged breakwater model, which located at $x = 3.0$ m on the sloping bed, was a 10.0-cm crest wide rectangle cement blockwork. The height of emergence d was 0.0 cm, 5.0 cm and 10.0 cm respectively.

Seven WG-50 capacitance wave gauges (Canadian RBR Limited Liability Company) and four AWMS ultrasonic water-level gauges (Beijing Sinfotek Science and Technology Co., Ltd) were used to measure the wave surface elevations at selected locations shown in Fig. 1. The wave gauges (WG) were numbered from WG 1 to WG 7. Their locations (in the coordinate system defined in Fig. 1) were adjusted according to water depth. The

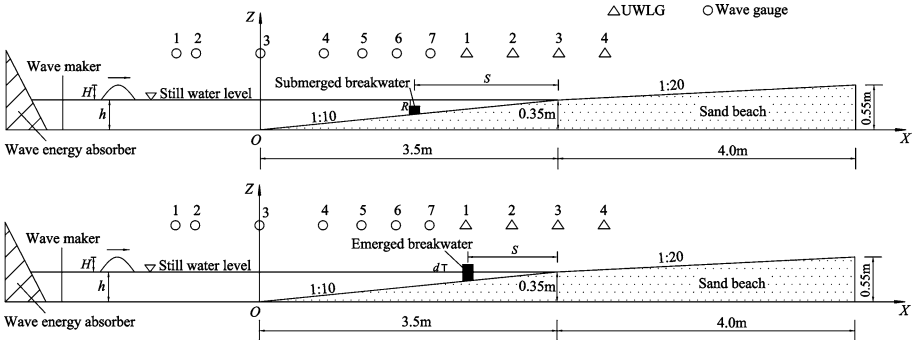

Fig. 1 Experimental setup: *top panel*—submerged breakwater; *bottom panel*—emerged breakwater

Table 1 Summary of test conditions

Type	Case	Water depth h (m)	Wave height H (m)	Offshore distance of breakwater S (m)	Depth of submergence R (cm)	Height of emergence d (cm)
Submerged breakwater	1	0.35	0.15	1.75	5.0	–
	2	0.35	0.15	1.50	5.0	–
	3	0.35	0.15	1.25	5.0	–
	4	0.35	0.15	1.00	5.0	–
	5	0.35	0.15	1.50	8.0	–
	6	0.35	0.15	1.50	10.0	–
Emerged breakwater	7	0.35	0.15	0.50	–	0.0
	8	0.35	0.15	0.50	–	5.0
	9	0.35	0.15	0.50	–	10.0
Without breakwater	10	0.35	0.15	–	–	–

surface elevations were sampled at 50 Hz. The ultrasonic water-level gauges (UWLG) numbered from UWLG 1 to UWLG 4 were positioned at certain specified distances above the still water level. The water levels were sampled at 20 Hz.

The beach profile change after wave run was measured using the URI-IIU ultrasonic topographic meter (UTM, Wuhan University Electronic Information Institute, China), which has measurement accuracy up to ± 1 mm.

One camera (Logitech C910 HD Webcam with a resolution of 1MP) was located at one side of the wave flume to provide a side view of such processes as wave uprush and backwash processes, sediment movement, and beach profile changes. The frame rate of camera was fixed at 15 Hz. Grid lines were also marked on the front side of the glass wall for extracting from the images recorded by the camera such information as waveform, flow depths, and instantaneous erosion and deposition depths. The distance between two adjacent grid lines was 5 cm in both the vertical and horizontal directions. The locations of camera needed to be slightly adjusted for each case.

The Vectrino three-dimensional acoustic Doppler velocimeter (Norway Nortek AS) was used to measure the single-point water velocity for numerical model validation. Data collection frequency was set to 100 Hz.

A detailed description of the preparation and measurement of wave surface elevations and bed profiles can be found in Chen et al. (2012), and only the key steps are summarized in the following for completeness.

Before test, some repeatability studies in the experiment were carried out including solitary wave generating, preparation of initial beach profile, and beach profile changes under the same wave condition. The repeatability of wave maker in the experiment was satisfactory, and the maximum deviation was <3 %. The maximum deviation of twice beach profile changes in the same situation was <0.2 cm. The overall agreement in the experiment was satisfactory.

Before each test, the flume was first filled slowly with water to the desired water depth, and then the sandy beach was allowed to soak for more than 12 h. Bed profiles were measured using a URI-IIU ultrasonic topographic meter. The initial bed profile was measured along two cross-shore sections ($y = 16.50$ and 31.50 cm, see Fig. 1 for the definition of the coordinate system). To minimize possible random measurement errors, the

bed profile was all measured twice along each cross-shore section. For each test condition, the measured bed profile is the average of four measurements. The same wave condition was run 15 times (labeled as 1 wave to 15 waves in the figures presented in this paper) to study the evolution of bed profile and scour around breakwater. After collecting data in one test condition, the sand beach was rebuilt with the same well-mixed sand.

3 Model validation

The governing equations of three-dimensional model are Navier-Stokes equations in FLOW-3D. The Reynolds stress terms are closed by RNG k-ε turbulence models. The volume-of-fluid (VOF) method is employed for free surface trace. FLOW-3D numerically solves the equations described using finite-difference approximations. The flow region is subdivided into a mesh of fixed rectangular cells. Description and applications of FLOW-3D can be found in its user manual (2009).

The proposed FLOW-3D was examined by comparison with two cases experimental results. Figures 2 and 3 demonstrate comparisons between the numerical and experimental results for the wave free surface elevations and single-point flow velocities in case 7 and case 10 respectively. These indicate that the overall agreement between experimental and numerical results is good, and FLOW-3D is able to satisfactorily reproduce the flow velocities of tsunami wave.

4 Results and discussions

4.1 Submerged breakwater

The initial bed profile and those after running waves under the effect of submerged breakwater are plotted in Fig. 4a–f for case 1-6, and the comparison of normalized elevation change (bed elevation changes ΔZ/wave height H) with and without submerged breakwater is also given in Fig. 4a–f. Based on the data collected by UTM, as well as video recordings in camera, the tsunami wave plunging on the thin layer of water prior to reaching the shoreline not entrains much sediment. The wave runs up to the maximum and then runs down toward seaward. The back wash flow velocity is high, and the water depth is shallow with high sediment concentration, which resulted in net erosion of this region. As the flow with high concentration of sediment injects into the bottom of the run-down jump, a large recirculation region is formed by the same process which leads to the run-down jump. The sudden deceleration of the sediment-rich seaward flow, as well as the long particle residence time caused by the recirculation region, allows the sediments to deposit in this region. Consequently, a large net deposit zone is observed in the recirculation region.

For each case, erosion on the shore face and deposition offshore are found; the erosion and deposition depths increase with increasing number of attacking waves, and it could be expected that an equilibrium profile could be reached after running enough number of waves. Our observations agree with the observations of Kobayashi and Lawrence (2004), Young et al. (2010), and Chen et al. (2012), who found in their experiments that the strong backwash water could cause erosion on the foreshore and a deposition seaward of the shoreline. The only two differences are that the deposition depth and location changes, and there is a scour hole near submerged breakwater. The experimental results show that the

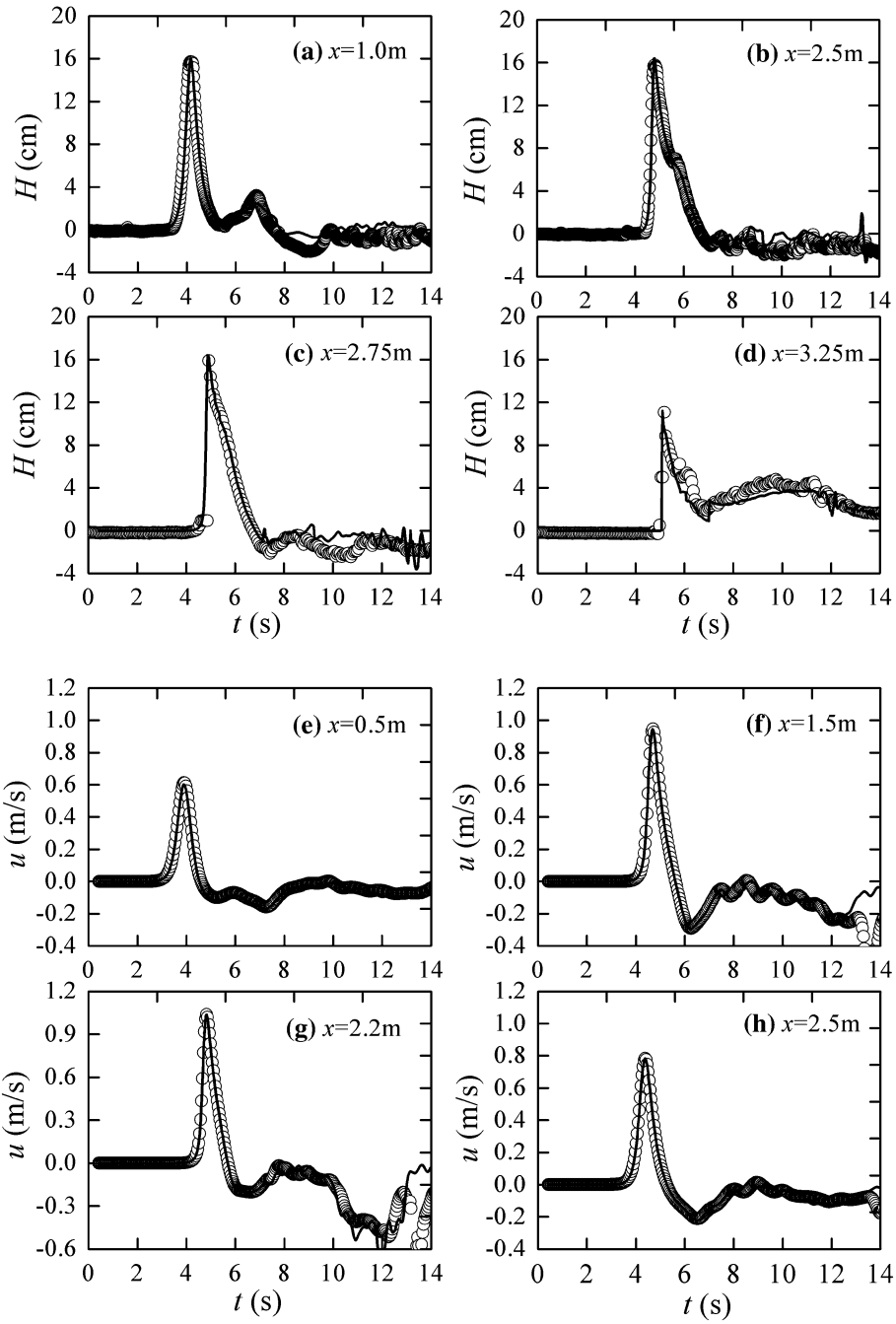

Fig. 2 The wave free surface elevations and single-point flow velocities predicted by numerical model and experimental measurement in case 7. The *solid line* represents the numerical results and the *points* represent experimental data

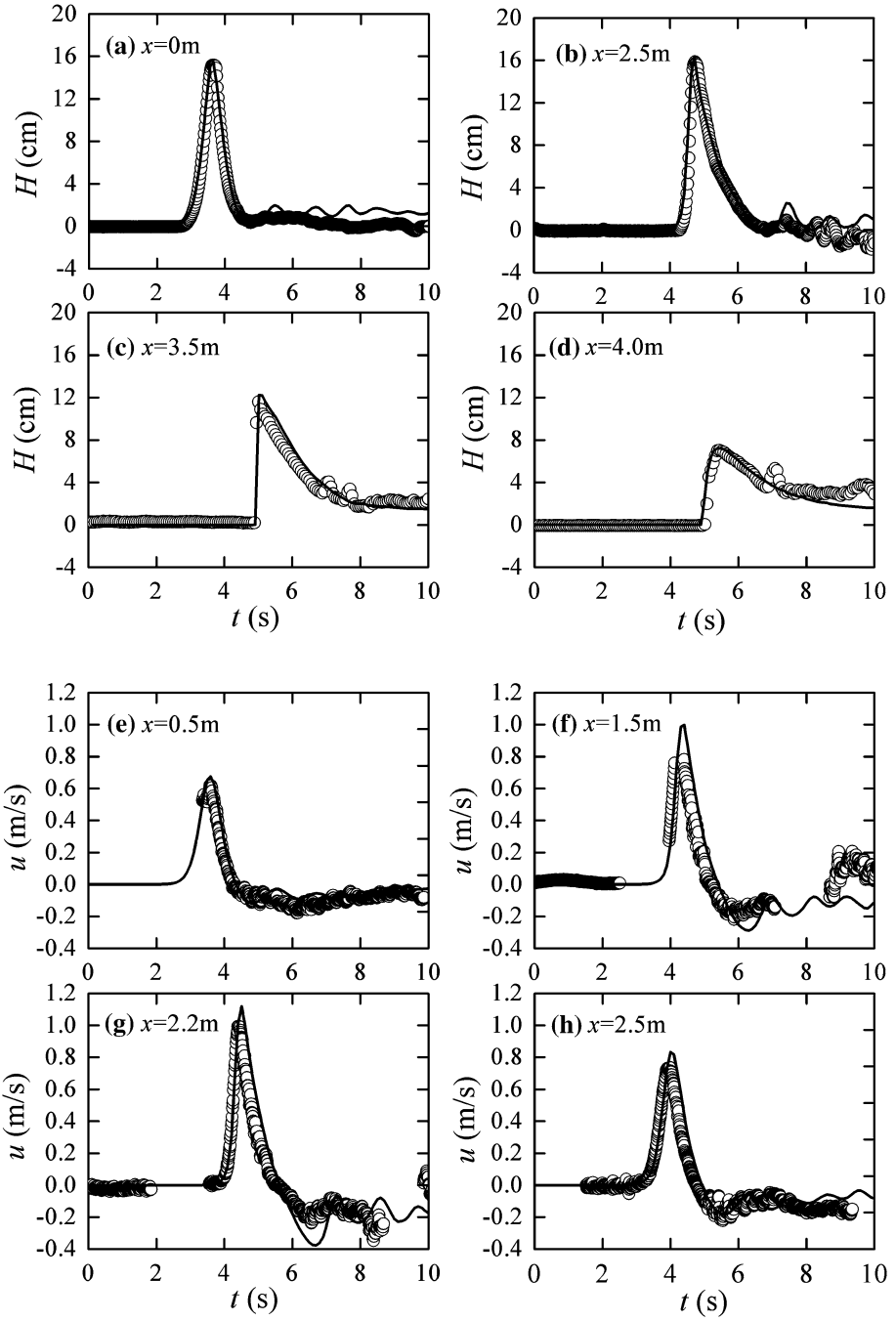

Fig. 3 The wave free surface elevations and single-point flow velocities predicted by numerical model and experimental measurement in case 10. The *solid line* represents the numerical results and the *points* represent experimental data

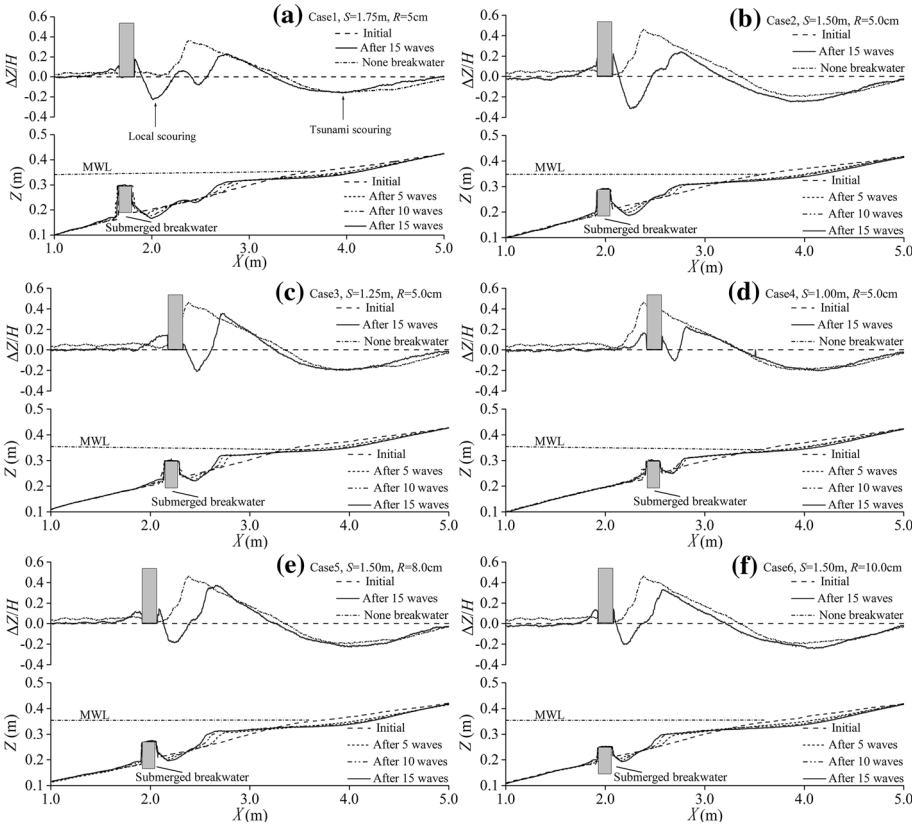

Fig. 4 Bed profiles and bed profile changes affected by submerged breakwater after from one to fifteen waves

submerged breakwater could not effectively reduce the tsunami scouring on the sandy beach. The submerged breakwater may only influence the height and position of deposition sand bar. The height of deposition sand bar decreases in the same depth of submergence R, as the location of submerged breakwater S decreases. As shown in Fig. 4d, the effect of reducing the deposition sand bar could be obvious when the submerged breakwater is located in where the run-down jump took place. As shown in Fig. 4c, when submerged breakwater is located near the run-down jump zone, breakwater restricts run-down jump, and sediments deposit in this region. So the maximal value of height of deposition sand bar occurs.

The location of maximum deposition sand bar moves to seaward as depth of submergence increases; meanwhile, there are no regular changes of the height of deposition sand bar. The height of deposition when depth of submergence $R = 8.0$ cm is greater than that when depth of submergence $R = 5.0$ cm and 10.0 cm. The erosion and deposition of the beach mainly occur in two stages according to the video recording. The tsunami wave goes over the breakwater, and the breaking wave has a scouring effect on the beach in uprush process. The erosion also is caused mainly by backwash sheet flows. Meanwhile, there is a deposition on the seaward of submerged breakwater and a scouring on the shoreward. The deposition sand bar could obvious reduce when the submerged breakwater locate in the run-down jump took

place. The maximum local tsunami scour depth could decrease, as depth of submergence changes and offshore distance of submerged breakwater decreased.

4.2 Emerged breakwater

The initial bed profile and those after running several waves are plotted in Fig. 5a for Case 7. The local scour is observed in a large area shoreward of the emerged breakwater as well as in a region immediately seaward of the breakwater. The erosion shoreward of the breakwater evolves with the number of attaching waves into a deep scour hole, but the erosion seaward of the breakwater almost achieves equilibrium profile after fifth wave. For this test condition, the maximum scour depth in two sides of the breakwater reaches about 6.0 cm. Meanwhile a deposition sand bar about 5.1 cm is formed in seaward of the breakwater mainly due to the run-down jumps caused by the clasping of the retreating water and the waves in the undulating tails.

The initial bed profile and those after running several waves are plotted in Fig. 5b, c for the other two test conditions. Again, the local scour on the seaward and shoreward side of the breakwater is evident, and the erosion depth on shoreward of the breakwater increased with increasing number of attacking waves and on seaward of the breakwater reaches the equilibrium profile after fifth wave for all cases. The only difference is deposition depth change. The deposition sand bar is about 4.2 cm for case 8 and about 1.6 cm for case 9.

Information on bed elevation changes ΔZ in cases 7–9 and without emerged breakwater in case 10 is shown in Fig. 5d. If there is no emerged breakwater in the beach, the experimental result shows that there is a significant portion of scouring which results in erosion on the shoreface and sand deposition immediately seaward resulting in a large deposit region offshore. In contrast, if there is emerged breakwater, the beach is significantly protected by emerged breakwater, and the tsunami scouring rapidly decreases and almost does not appear. Meanwhile, there is a local scouring on the seaward and shoreward of the emerged breakwater. And there still is sand deposit on the seaward of breakwater. In shoreward of the emerged breakwater, the maximum depths of local scour are 5.9 cm, 4.4 cm, and 5.2 cm, respectively, in cases 7–9. The relationship between the maximum depths of local scour and height of emergence d shows very weak correlation. In seaward of the emerged breakwater, the maximum depths of local scour are 6.4 cm, 3.9 cm, and 2.5 cm, respectively, in cases 7–9, which decreases as height of emergence d increases. And the height of sand deposit in the seaward of the emerged breakwater decreases as height of emergence d increases. The result shows that the height of sand deposit declines 24 %, when height of emergence d increases twofold.

Figures 6, 7, and 8 give the numerical simulation of flow and vorticity fields on first tsunami wave over the emerged breakwater in cases 7–9 respectively, including uprush process (as shown in Figs. 6a, 7a, 8a) and backwash process (as shown in Fig. 6b, 7b, 8b). Figure 6a, 7a, and 8a show that the wave overs the emerged breakwater and then rushes up onto the beach as a moving bore with high velocity and accompanies the vortex near the toe, which has a local scouring effect on shoreward of the emerged breakwater. The uprush flow with high velocity and vortex works together to cause scour hole near the toe. The maximum uprush velocity appears on case 7, that is the height of emergence d is lowest. So the uprush flow can easy to over the breakwater then carry amount of sand form the bed caused scour hole near the toe. The maximum vorticity appears on case 9, that is the height of emergence d is highest. In the case that the crown height of a breakwater is fairly high compared with the thickness of a uprush flow, the flow separates from crown of breakwater and then draws a parabolic curve as shown in Fig. 8a. The uprush flow associated with

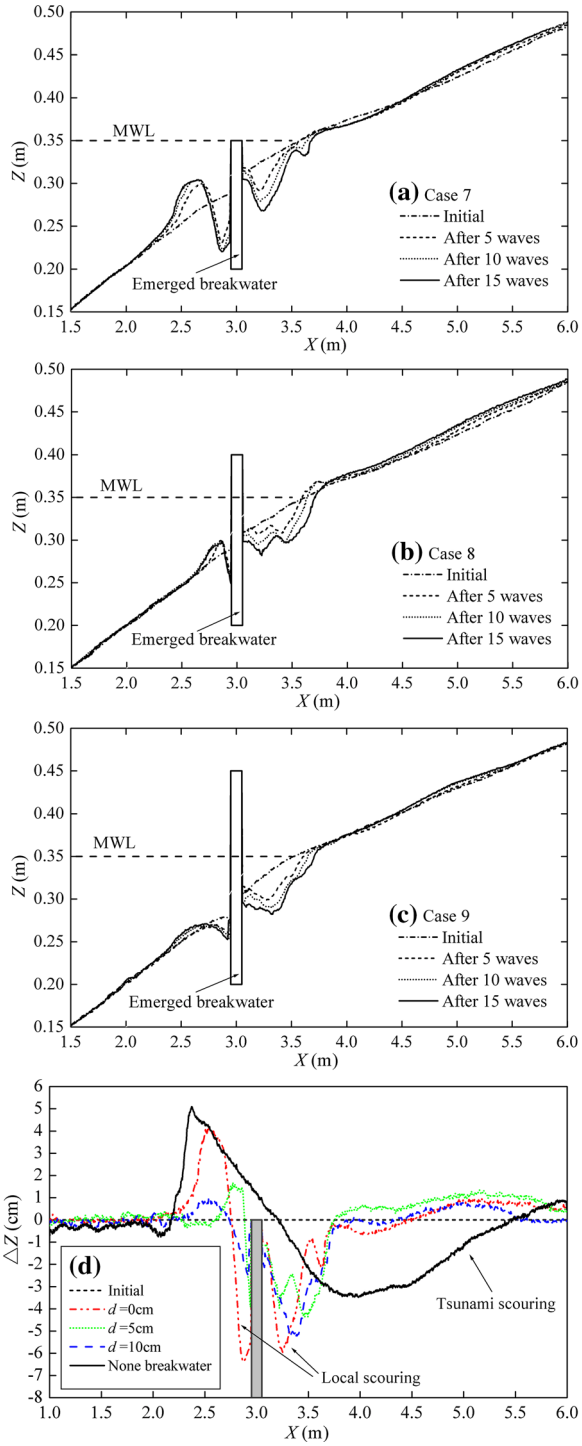

Fig. 5 Bed profiles and bed profile changes affected by emerged breakwater after from one to fifteen waves

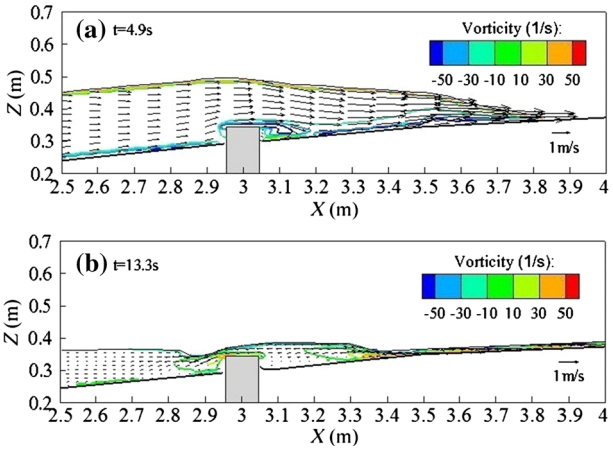

Fig. 6 Numerical simulation of flow and vorticity fields on first tsunami wave over the emerged breakwater in case 7

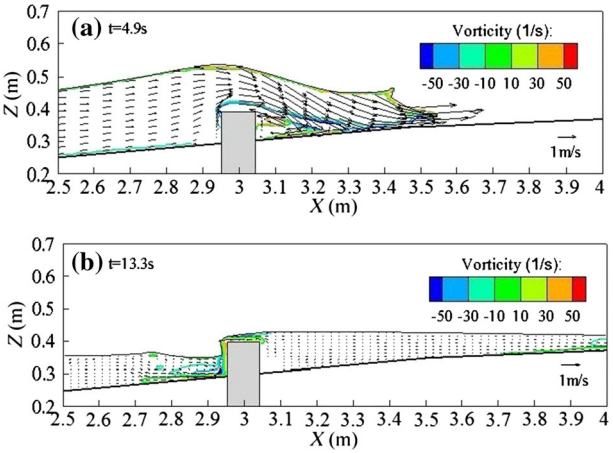

Fig. 7 Numerical simulation of flow and vorticity fields on first tsunami wave over the emerged breakwater in case 8

highly turbulent and vortex causes scour hole near the toe then tumbles in the scour hole. So the scour depth near the breakwater rapidly increases. Our above analyses agree with the experimental result of Fig. 5d, which found that the minimum depths of local scour in shoreward of the emerged breakwater appear in appropriate height of emergence d.

Figures 6b, 7b, and 8b show that the back-flow separates from the crown of the breakwater and drops into bed as plunging jet. The jet causes the local scour in seaward of the emerged breakwater. The backflow could be blocked by emerged breakwater with high crown. When the emerged breakwater has low crown, the strong water jet could cause scour hole near the toe and then further rapid increase the scour depth by suspending sand from the scour hole and carrying the suspended sand downstream of the breakwater, resulting in a deposit region offshore. These can be explained by the result of Fig. 5d, in which depth of local scour in seaward decreases as height of emergence d increases.

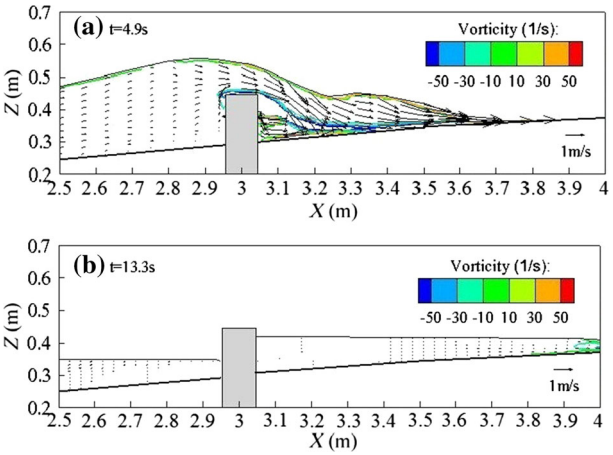

Fig. 8 Numerical simulation of flow and vorticity fields on first tsunami wave over the emerged breakwater in case 9

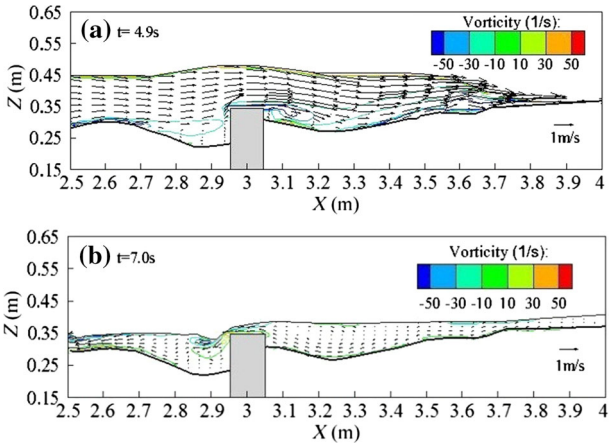

Fig. 9 Numerical simulation of flow and vorticity fields on fifteenth tsunami wave over the emerged breakwater in case 7

Figure 9 gives the numerical simulation of flow and vorticity fields when 15th tsunami wave over the emerged breakwater on the eroded bed in case 7. The local scours are observed in seaward and shoreward of the emerged breakwater and sand deposit is observed in a region immediately seaward of the breakwater. As shown in Fig. 9a, the 15th wave overs the breakwater and rushes up onto the beach with lower velocity compared with first wave (as shown in Fig. 6a). The up-rush flow also accompanies strong vortex, which further increased the scour depth. The scour depth of shoreward of emerged breakwater is not likely to reach its equilibrium stage for typical tsunamis. The backflow through breakwater and drops into bed with lower velocity. The scour hole on the seaward of the emerged breakwater nearly reaches the equilibrium profile.

The experimental results show that emerged breakwater could significantly effectively reduce the tsunami scouring on the sandy beach, and submerged breakwater could not. The

most of wave energy is concentrated in crest of solitary wave. The wave could smoothly overs the submerged breakwater, neither produces the reflection or break. The strong downrushing water causes tsunami scouring on the foreshore. Therefore, the submerged breakwater could not effectively reduce the tsunami scouring. While run-down jump could be affected by submerged breakwater, the height and position of deposition change with the depth of submergence R and location of submerged breakwater S. The emerged breakwater blocks tsunamis invasion and significantly protects the sandy beach; meanwhile, respective induced plunging jet in uprush and backwash process caused local scouring on both sides. The information reported in this study is useful for local authorities to assess potential tsunami damage and to have a better plan for tsunami disaster preventing and reducing.

4.3 Local scouring

Local scouring damage is one of the main factors leading to the destruction of coastal structures during a tsunami event. The local scouring around the breakwater is the functions of the combination of wave, sediment, and breakwater parameters. As a result, the general functional expressions representing an event related to the effect of breakwater on magnitude and position of local scouring are

$$f(z_{\max}, H, d_{50}, B, d_w, h_1, S, L) = 0 \tag{1}$$

$$f(D_s, H, d_{50}, B, d_w, h_1, S, L) = 0 \tag{2}$$

As shown in Fig. 10, $Z_{\max}$ is the maximum depth of local scouring; D_s is the distance of $Z_{\max}$ location from breakwater; H is the incident wave height; d_{50} is the mean median diameter of sand; B is the crest wide of breakwater; d_w is the height of breakwater; h_1 is the water depth in breakwater; if $d_w < h_1$, it is the submerged breakwater; if $d_w > h_1$, it is the emerged breakwater; S is the offshore distance of breakwater; L is the length between the slope starting point and water-land boundary.

Because of the larger number of parameters in Eqs. (1) and (2), it is necessary to simplify the analysis by making use of the dimensional properties of the various parameters; this result in

$$\Pi = f\left(\frac{z_{\max}}{B}, \frac{H}{d_{50}}, \frac{d_w}{h_1}, \frac{S}{L}\right) \tag{3}$$

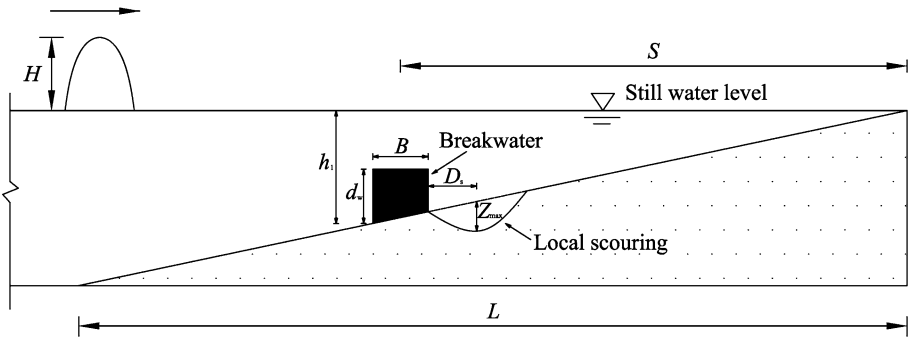

Fig. 10 Schematic representation of breakwater and local scouring

$$\Pi = f\left(\frac{D_s}{B}, \frac{H}{d_{50}}, \frac{d_w}{h_1}, \frac{S}{L}\right) \tag{4}$$

In the above equation $\frac{z_{max}}{B}$ is the dimensionless magnitude of local scouring parameter; $\frac{D_s}{B}$ is the dimensionless position of local scouring parameter; $\frac{H}{d_{50}}$ is the dimensionless magnitude of wave height parameter; $\frac{d_w}{h_1}$ is the dimensionless magnitude of breakwater parameter; $\frac{S}{L}$ is the dimensionless position of breakwater parameter.

The final empirical relation that defines the magnitude of local scouring around the breakwater given as

$$\frac{z_{\max}}{B} = 0.001\left(\frac{S}{L}\right)^{0.385}\left(\frac{H}{d_{50}}\right)\ln\left(\frac{d_w}{h_1}\right) + 0.426 \tag{5}$$

With a coefficient of determination equal to 0.465, the relation between the empirical equation and the dimensionless parameters is given in Fig. 11(a). The results show that local scouring is affected by hydrodynamic intensity, size and position of breakwater. The

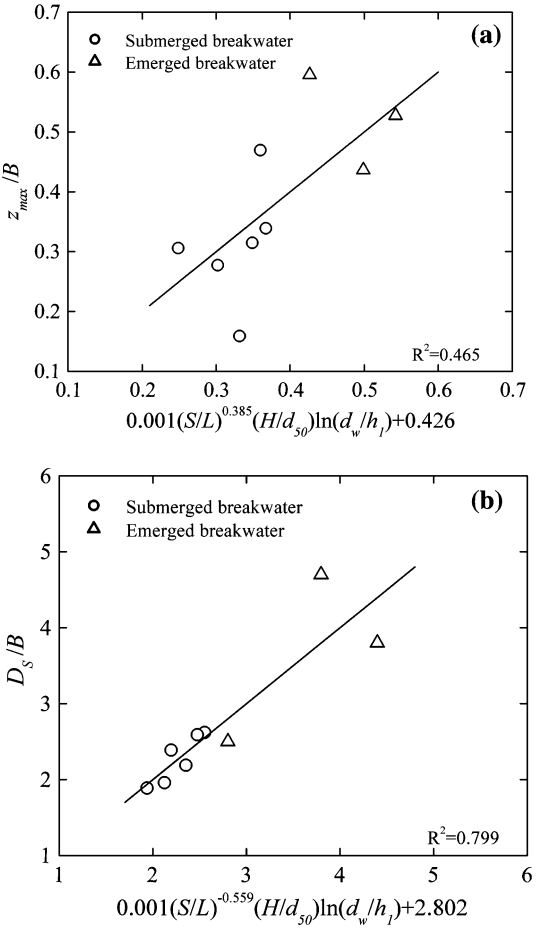

Fig. 11 Dimensionless trend of the maximum local scour (Z_{max}) and distance of Z_{max} location from the breakwater (D_s)

maximum depths of local scouring increases as wave height, height of breakwater, and offshore distance of breakwater increases.

The final empirical relation that defines the position of local scouring around the breakwater is given as

$$\frac{D_s}{B} = 0.001\left(\frac{S}{L}\right)^{-0.559}\left(\frac{H}{d_{50}}\right)\ln\left(\frac{d_w}{h_1}\right) + 2.802 \tag{6}$$

Above empirical definition follows a relationship possessing good trend between the dimensionless parameters. The coefficient of determination, R^2, between the dimensionless parameters is 79.9 % (Fig. 11b). The results show that location of local scouring is also affected by hydrodynamic intensity, size and position of breakwater. The distance of Z_{max} location from breakwater increases as wave height, height of breakwater increases, and offshore distance of breakwater decreases.

According to Eqs. (5) and (6), the maximum depth of local scouring Z_{max} is 5.6 cm and the distance of Z_{max} location from emerged breakwater D_s is 36.4 cm for case 8 (emerged breakwater; height of emergence $d = 5$ cm; incident wave height $H = 15$ cm; offshore distance of breakwater $S = 0.5$ m), as shown in Fig. 12. If we increase incident wave height H, such as incident wave height $H = 20$ cm for case 8, we could predict that Z_{max} is 6.04 cm and D_s is 39.2 cm. If we increase height of emergence d, such as height of emergence $d = 15$ cm for case 8, we could predict that Z_{max} is 6.93 cm and D_s is 44.8 cm. If we increase offshore distance of breakwater S, such as offshore distance of breakwater

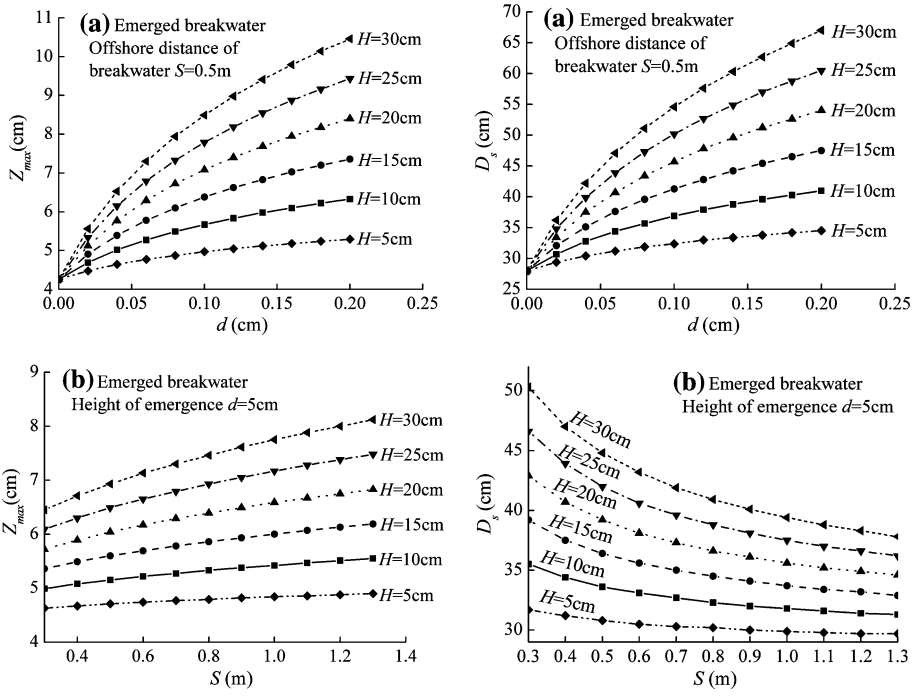

Fig. 12 Variation of maximum local scour (Z_{max}) and distance of Z_{max} location from the emerged breakwater (D_s) with height of emergence d, incident wave height H and offshore distance of breakwater S

$S = 1.0$ m for case 8, we could predict that Z_{max} is 6.0 cm and D_s is 33.7 cm. As shown in Fig. 12, the results indicate that the maximum depth of local scouring Z_{max} increases as incident wave height H, height of emergence d, and offshore distance of breakwater S increase. The distance of Z_{max} location from emerged breakwater D_s increases as incident wave height H, height of emergence d increases, and the offshore distance of breakwater S decreases.

5 Concluding remarks

The protection capabilities of tsunami scour by offshore submerged or emerged breakwater are studied experimentally, and the following conclusions can be drawn from our experimental results.

1. The submerged breakwater could not effectively reduce the tsunami scouring and only could affect the height and position of deposition sand bar.
2. The emerged breakwater could significantly effectively reduce the tsunami scouring on the sandy beach. Local scour could occur mainly on the both side of the structure at the same time.
3. The plunging jet, which due to flow is separated from the crown and drops into bed, causes the local scour in both side of the emerged breakwater. The scour depth at shoreward is not likely to reach its equilibrium stage for typical tsunamis. Attention should be given when designing measures to protect the breakwater.
4. The most important governing parameters on local scouring around breakwater were defined. These parameters were written as a dimensionless group, and based upon the experimental data empirical, equations were developed. The final empirical relations that define the magnitude and position of local scouring around the breakwater were presented.
5. The maximum depths of local scouring Z_{max} increases as wave height, height of breakwater and offshore distance of breakwater increases. The distance of Z_{max} location from breakwater increases as wave height, height of breakwater increases, and offshore distance of breakwater decreases.

There are many engineering structures in located in coastal zone to prevent the coastal erosion under storm events, such as groins, artificial headland, and revetment. Further research is needed to study how to provide protection for tsunami scour by other engineering structures and how to estimate potential structures damage for local authorities to better plan for tsunami disaster preventing and reducing.

Acknowledgments The study is financially supported by the National Natural Science Foundation of China (Nos. 51239001 and 51409022) and the Scientific Research Fund of Hunan Provincial Education Department (Nos. 13B130 and YB2015B034). Partial support also comes from the Program for Ministry of Communications Key Laboratory of Port, Waterway and Sedimentation Engineering and the Graduate Student Research Innovation Project of Hunan Province (No. CX2015B360).

References

Alsina JM, Falchetti S, Baldock TE (2009) Measurements and modelling of the advection of suspended sediment in the swash zone by solitary waves. Coast Eng 56(5–6):621–631

Ca V, Yamamoto Y, Charusrojthanadech N (2000) Improvement of prediction methods of coastal scour and erosion due to Tsunami back-flow. In: Proceedings of the twentieth international offshore and polar engineering conference, Beijing, PR China, pp 1053–1062

Chen J, Huang ZH, Jiang CB, Deng B, Long YN (2012) An experimental study of changes of beach profile and mean grain size caused by tsunami-like waves. J Coast Res 28(5):1303–1312

Chen J, Huang ZH, Jiang CB, Deng B, Long YN (2013) Tsunami-induced scour at coastal roadways: a laboratory study. Nat Hazards 69:655–674

Dean RG, Dalrymple RA (2001) Coastal Processes with Engineering Applications. Cambridge University Press, Cambridge

Flow Science Inc (2009) FLOW-3D user manual version 9.4. Flow Science Inc, Santa Fe, New Mexico, USA

Goring DG (1979) Tsunamis-the propagation of long waves on to a shelf. California Institute of Technology, Pasadena

Jiang CB, Chen J, Yao Y, Liu J, Deng Y (2015) Study on threshold motion of sediment and bedload transport by tsunami waves. Ocean Eng 100:97–106

Kato F, Sato S, Yeh H (2000) Large-scale experiment on dynamic response of sand bed around a cylinder due to tsunami. In: Proceedings of 27th international conference on coastal engineering, ASCE, Sydney, Australia, pp. 1848–1859

Kobayashi N, Lawrence A (2004) Cross-shore sediment transport under breaking solitary waves. J Geophys Res 109:C030047

Li L, Huang Z, Qui Q, Natawidjaja DH, Sieh K (2012) Tsunami-induced coastal change: scenario studies for Painan, West Sumatra, Indonesia. Earth Planets Space 64:799–816

Madsen PA, Fuhrman DR, Schaeffer HA (2008) On the solitary wave paradigm for tsunamis. J Geophys Res. doi:10.1029/2008jc004932

Nakamura T, Kuramitsu Y, Mizutani N (2008) Tsunami scour around a square structure. Coast Eng J 50(2):209–246

Nakamura T, Mizutani N, Yim SC (2009) A three-dimensional coupled fluid-sediment interaction model with bed-load/suspended-load transport for scour analysis around a fixed structure. J Offshore Mech Arctic Eng ASME 131(3):031104-1–031104-9

Seiji WN, Uda T, Tanaka S (1987) Statistical study on the effect and stability of detached breakwaters. Coast Eng Jpn 30(1):121–131

Sumer BM, Sen MB, Karagali I, Ceren B, Fredse J, Sottile M, Zilioli L, Fuhrman DR (2011) Flow and sediment transport induced by a plunging solitary wave. J Geophys Res 116:C01008

Synolakis CE, Bernard EN (2006) Tsunami science before and beyond Boxing Day 2004. Philos Trans A Math Phys Eng Sci 364(1845):2231–2265

Tonkin S, Yeh H, Kato F, Sato S (2003) Tsunami scour around a cylinder. J Fluid Mech 496:165–192

Tsujimoto G, Yamada F, Kakinoki T (2008) Time-space variation and spectral evolution of sandy beach profiles under tsunami and regular waves. In: Proceedings of the International Offshore and Polar Engineering Conference, Vancouver, BC, Canada, ISOPE, July 6–11, pp. 523–527

Young YL, Xiao H, Maddux TB (2010) Hyro- and morpho-dynamic modeling of breaking solitary waves over sand beach. Part I: experimental study. Mar Geol 269:107–118